Applied Surface Science 519 (2020) 146251

Contents lists available at ScienceDirect

Applied Surface Science

journal homepage: www.elsevier.com/locate/apsusc

Full Length Article

Intrinsic-strain-induced curling of free-standing two-dimensional Janus MoSSe quantum dots

Han Ye[a,b,*], Yunzhen Zhang[a], Anran Wei[c], Delong Han[a], Yumin Liu[a], Wenjun Liu[a], Yuefeng Yin[b], Mingchao Wang[b,*]

[a] State Key Laboratory of Information Photonics and Optical Communications, Beijing University of Posts and Telecommunications, Beijing 100876, China
[b] Department of Materials Science and Engineering, Monash University, Clayton, VIC 3800, Australia
[c] Department of Engineering Mechanics, School of Naval Architecture, Ocean and Civil Engineering, Shanghai Jiao Tong University, Shanghai 200240, China

ARTICLE INFO

Keywords:
Janus transition metal dichalcogenides
Quantum dot
Intrinsic strain
Molecular dynamics
Finite element method

ABSTRACT

Motivated by the fascinating properties of both two-dimensional transition metal dichalcogenide quantum dots (TMD QDs) and Janus TMD monolayers, we theoretically explore the equilibrium structures of free-standing Janus MoSSe QDs in which atomic asymmetry of chalcogen is introduced. Two distinct types of spontaneous curling are observed by molecular dynamics simulations, and the curling behavior depends on the size of QD. The bowl-like (tube-like) curling occurs in relatively small (large) MoSSe QDs with different shapes (hexagon and triangle) and edge types (zigzag and armchair). The transition between these two curling types occurs at the sizes of around 10 nm and 13 nm for hexagonal and triangular shapes, respectively. By applying equivalent misfit strains into two adjacent sublayers, finite element analysis reproduces similar curling behavior. This confirms the relaxation of intrinsic strain in Janus structure acting as the predominant driving force of spontaneous curling. In addition, the curvatures of Janus TMD QDs increase from MoSSe to MoSeTe to MoSTe, indicating the positive correlation between the curling and misfit.

1. Introduction

Beyond graphene, two-dimensional transition metal dichalcogenides (2D TMDs) with tunable bandgaps have attracted huge interest in pursuit of their appealing physical and chemical properties [1–3]. By reducing the lateral size down to tens of nanometers and even smaller, fascinating properties arise in the 2D TMD quantum dots (QDs) due to the edge and quantum confinement effects, which provide superior applications in catalysis [4–6], biological sensing and imaging [7–9], optoelectronic devices [10] and so on. In experiments, synthesis of TMD QDs has been successfully achieved by various approaches, including mechanical and intercalation-assisted exfoliation [11–14], hydrothermal and solvothermal reaction [15,16], chemical vapor deposition (CVD) [17] and laser pulse ablation [18,19]. The common size of synthesized TMD QDs falls in the range from 2 nm to 20 nm [7]. The crystal structures are found dominantly 2H phase with semiconducting nature [20], while intercalation-assisted exfoliation (e.g. Li, K, H^+) may introduce a transition from 2H phase to metallic 1T phase [9,21]. In comparison with 2D TMD monolayers, the bandgaps of 2H phase TMD QDs are much larger due to the quantum confinement effects [9], and also influenced by edges, defects and dopants introduced during the synthesis process [22]. If forming a lateral heterostructure (i.e. MoS_2/WS_2, MoSe2/WSe2), the embedded TMD QD with proper size has been theoretically predicted as ideal system for confining massive Dirac fermions [23].

The atomic asymmetry of chalcogen in Janus MXY (M = Mo, W or Nb; X/Y = S, Se, or Te, X ≠ Y) monolayer brings unique properties. Recently, a presentative Janus TMD monolayer, MoSSe, has been experimentally synthesized via two strategies. Lu et al. [24] adopted a two steps approach: single-crystalline MoS_2 was treated by hydrogen plasma to generate fully hydrogenated MoS, then selenized the MoSH at a proper temperature between 350 and 450 °C. Alternatively, Zhang et al. [25] sulfurized the top Se atomic layer of the CVD-prepared $MoSe_2$ on SiO_2 at 800 °C while entirely retaining the underlying Se atomic layer. The improvement of hydrogen evolution reaction (HER) catalytic activity on the basal plane of Janus TMD monolayer has been theoretically predicted by density functional theory (DFT) calculations [26,27] and experimentally observed in MoSSe monolayer [25]. Moreover, Janus TMD monolayer possesses an out-of-plane piezoelectric polarization induced by uniaxial strain in basal plane which is

* Corresponding authors at: State Key Laboratory of Information Photonics and Optical Communications, Beijing University of Posts and Telecommunications, Beijing 100876, China (H. Ye).
E-mail addresses: Han_ye@bupt.edu.cn (H. Ye), Mingchao.wang@monash.edu (M. Wang).

https://doi.org/10.1016/j.apsusc.2020.146251
Received 18 January 2020; Received in revised form 21 February 2020; Accepted 28 March 2020
Available online 31 March 2020
0169-4332/

absent in MX_2 monolayer. Interestingly, much stronger out-of-plane piezoelectric polarization can be induced by vertical strain applied to stacked multilayers [28]. Motivated by the fascinating properties shown in both 2D TMD QDs and Janus TMD monolayers, we intentionally introduce atomic asymmetry of chalcogen in QD to form Janus MoSSe QDs, and conduct both molecular dynamics (MD) simulations and finite element (FE) analysis to explore their equilibrium structures and the driving forces for the morphology transition.

2. Modeling and simulations

DFT calculations of Janus MoSSe monolayer are carried out using the Vienna *ab initio* simulation package (VASP) with projector augmented wave (PAW) potentials [29,30]. The exchange-correlation functional is set the Perdew-Burke-Ernzerhof (PBE) form of the generalized gradient approximation (GGA) [31]. An energy cutoff of 520 eV is used for the plane-wave expansion of the electronic wave function and the energy convergence criterion is set 10^{-6} eV. The geometry optimization is implemented with the unit cell of Janus MoSSe monolayer with a 20 Å vacuum layer to avoid periodic interaction. The Brillouin zone for the unit cell is sampled with 17 × 17 × 1 k-points mesh with Monkhorst–Pack scheme [32] and the structures are fully relaxed until the forces on each atom are smaller than 0.01 eV/Å. The optimized lattice constant of Janus MoSSe monolayer is 3.25 Å (same as in Ref. [24]), falling between the lattice constants of MoS_2 (3.18 Å) and $MoSe_2$ (3.32 Å) monolayers. Other geometric parameters are listed in Table 1, and the results are in agreement with previous DFT studies [33]. Phonon dispersion analysis is performed by using the PHONOPY code and the force constants are determined by density-functional perturbation theory [34,35]. Calculated phonon dispersion of Janus MoSSe monolayer along high symmetry points is demonstrated in Fig. 1(c). There are 3 atoms in the primitive cell, allowing 9 phonon branches including 3 acoustic modes and 6 optical modes. No imaginary frequency is found around Γ point, indicating the structural stability of Janus MoSSe monolayer.

As the top view and side view shown in Fig. 1a and b, 2D Janus MoSSe QDs are constructed by the DFT optimized unit cell. Commonly observed hexagonal and triangular shapes [7,20,36] with zigzag and armchair edges are focused. For triangular QD, S/Se and Mo terminated zigzag edges are considered individually. The size of hexagonal (triangular) QD is measured by the length of diagonal line (length of edge). The considered size is set up to 25 nm, comparable with the experimentally obtained large 2D TMD QDs via exfoliation [7]. To explore the equilibrium structures of Janus MoSSe QD, we resort to MD simulations implemented by LAMMPS [37]. Recently developed Stillinger-Weber (SW) potential [38], applicable for various TMDs (MX_2, M = Mo, W; X = S, Se, Mo) and their alloy and lateral heterostructures, is adopted to describe the atomistic interactions in Janus TMDs. No specific constraint is applied, accounting for the free-standing condition. Starting from the flat configuration, the atoms in Janus MoSSe QD are allowed to relax using a conjugate gradient algorithm with a force tolerance of 10^{-10} eV/Angstrom. As a validation of the applied SW potential, the MD optimized structural parameters of Janus MoSSe monolayer are in agreement with the values obtained by DFT calculations (see in Table 1).

Table 1
Calculated lattice constant (a), heights of Mo-S layer ($h_{Mo\text{-}S}$) and Mo-Se layer ($h_{Mo\text{-}Se}$), bond lengths of Mo-S ($d_{Mo\text{-}S}$) and Mo-Se ($d_{Mo\text{-}Se}$), and bond angle ∠S-Mo-Se (θ) of Janus MoSSe. Values obtained from previous DFT study are also included for comparison.

	a (Å)	$h_{Mo\text{-}S}$ (Å)	$h_{Mo\text{-}Se}$ (Å)	$d_{Mo\text{-}S}$ (Å)	$d_{Mo\text{-}Se}$ (Å)	θ (°)
PBE	3.25	1.53	1.70	2.42	2.53	81.4
MD	3.223	1.54	1.67	2.41	2.50	81.5
PBE with vdW-DFT (optB86) [33]	3.23	1.54	1.71	2.41	2.58	81.2

3. Results and discussion

The atomistic structures of free-standing Janus MoSSe QDs after relaxation in MD simulations are exhibited in Fig. 2, taking representatively small and large QDs as examples. Two distinct types of spontaneous curling are observed. For small QDs with the size of around 4–5 nm, all corners of QDs roll up to exactly same extent, forming a bowl-like shape. For large QDs with the size of around 20 nm, the major rolling happens perpendicularly to one single axis, forming a mirror symmetric tube-like shape. The observed axis in hexagonal QD passes through the centers of two opposite edges, while this axis in triangular QD passes through one vertex and the center of its opposite edge. The quantitative criterion of curling type is to measure the distances between the vertexes of QDs. If no differences can be found, it belongs to the bowl-like curling. It is interesting that the same curling behavior is observed in QDs with both zigzag and armchair edges. The rolling axes are orthogonal to each other in these two cases. It means that no absolute preference of curling along zigzag or armchair exists in the hexagonal and triangular MoSSe QDs, unlike square MoSSe flake [39]. If the system is then thermalized (to 0.01 K and 298 K) and relaxed for 5 ns (1 fs a step) with Nose-Hoover thermostat and barostat (NVT) [40], we find vibration, distortion and rotation around the equilibrium shape, and the equilibrium shape repeatedly shows up during the simulation time. The temperature obviously determines the perturbation amplitudes but has little effect on the equilibrium state.

Such spontaneous curling behavior can be attributed to the atomic asymmetry in Janus TMD structures, since no buckling happens in the ordinary MoX_2 monolayer but their mismatched heterostructures [38]. In the unit cells optimized by both DFT and MD, it is clear that S and Se atoms are straightly aligned along vertical direction. The lateral lattice of MoSSe naturally falls between the values of MoS_2 and $MoSe_2$. If ordinary MoX_2 monolayer is considered as strain free, intrinsic strain exists in the MoXY monolayer due to the lattice misfit. In such case, Mo-S bond is intrinsically in tensile state, while Mo-Se bond is in compressive state. As a consequence, the relaxation of these intrinsic strains in free-standing Janus MoSSe QD results in their spontaneous curling (see Fig. 2).

Here, the mechanical properties of the Janus MoSSe monolayer along zigzag and armchair directions are calculated by MD. A 20 nm × 20 nm square flake with periodic boundary conditions is adopted. The uniaxial stress-strain curves and Poisson ratio-strain curves are plotted in Fig. 3a and b, respectively. In the linear range, the stress responses in two orthogonal directions are almost the same, while the stress along the zigzag direction becomes lower as the strain increases before fracture. For Poisson ratios, the values along two directions are almost identical at trivial tensile strain and then linearly decrease with different slopes as strain increases. The decreasing slope of Poisson ratio along armchair is larger. Since no external strain is intentionally applied to the free-standing QD, the Janus MoSSe can be reasonably regarded as an isotropic elastic material with Young's modulus E = 299 GPa (thickness is taken as $h_{Mo\text{-}S} + h_{Mo\text{-}Se}$) and Poisson ratio υ = 0.245, which are comparable with the reported values of TMDs [39,41]. The isotropic elastic response explains why the curvatures of QDs with similar sizes are not affected by the different edges, as shown in Fig. 2.

To further explicitly validate the origin of spontaneous curling of Janus MoSSe QD, we resort to FE analysis based on continuum elastic theory. The MoSSe monolayer is modeled by two adjacent sublayers. One sublayer stands for the Mo-S structure, while the other sublayer stands for Mo-Se. The heights of sublayers are $h_{Mo\text{-}S}$ and $h_{Mo\text{-}Se}$ as listed in Table 1, respectively. In FE model, equivalent misfit strains $\varepsilon_{Mo-S} = (a_{MoS_2} - a_{MoSSe})/a_{MoS_2}$ and $\varepsilon_{Mo-Se} = (a_{MoSe_2} - a_{MoSSe})/a_{MoSe_2}$ are imposed in the corresponding sublayer as the initial state. For

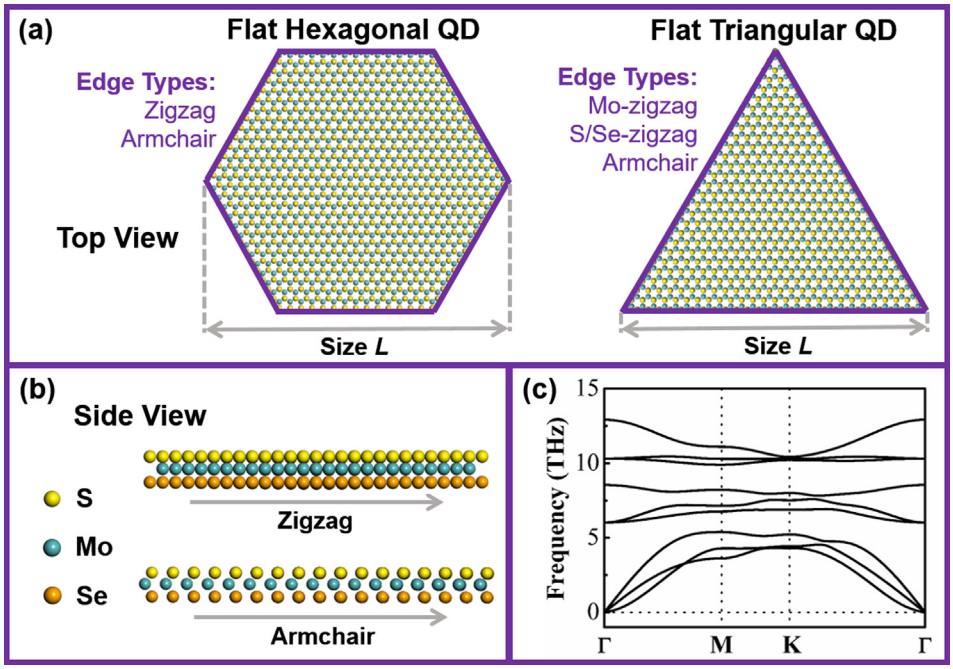

Fig. 1. (a) Schematic top view of hexagonal and triangular Janus MoSSe QDs. (b) Side view of edge along zigzag and armchair directions. (c) Phonon dispersion of Janus MoSSe monolayer.

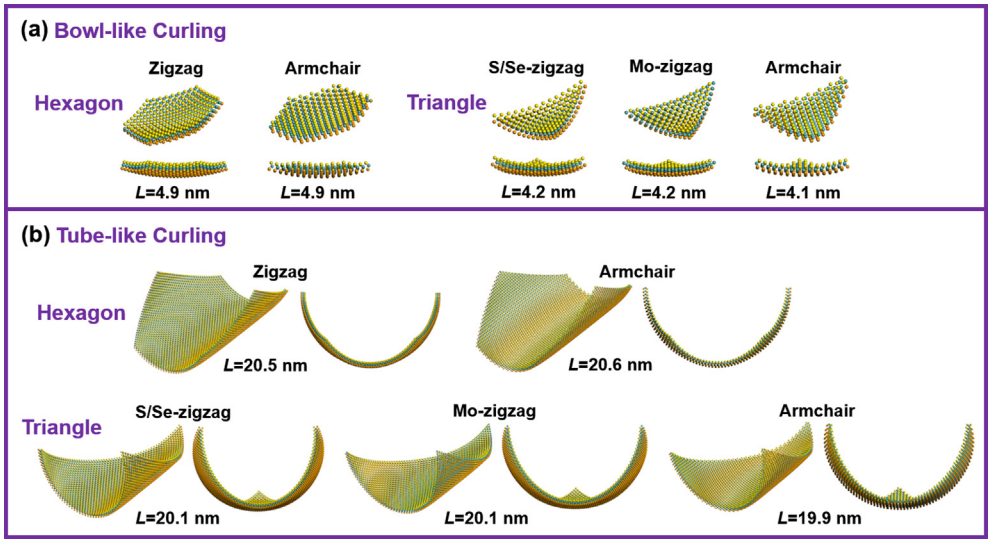

Fig. 2. (a) Bowl-like curling of small hexagonal and triangular Janus MoSSe QDs. Sizes of QDs are from 4 to 5 nm. (b) Tube-like curling of large hexagonal and triangular Janus MoSSe QDs. Sizes of QDs are around 20 nm.

simplicity, the MoSSe QD is treated as one-piece isotropic elastic material with Young's modulus and Poisson ratio obtained from MD. All edges of MoSSe QD are set as free boundaries. To make a comparison, the sizes of FE models are similar to the MD models shown in Fig. 2. After convergence, the FE solver provides the solution for equilibrium shape. As illustrated in Fig. 3, bowl-like curling happens in small hexagonal (L = 5 nm) and triangular (L = 4 nm) QDs, while tube-like curling happens in large (L = 20 nm) QDs. The FE analysis reproduces the curling behavior of Janus MoSSe QD in a satisfactory manner. The only discrepancy is the larger curvature in FE results. This qualitative agreement between atomistic simulations and continuum elastic theory confirms that the origin of spontaneous curling comes from the intrinsic strain induced by atomic asymmetry in Janus TMDs.

Taking hexagonal Janus MoSSe QD with zigzag edges as an example, Fig. 4a shows that a transition of curling type can be observed as the size of QD increases. When the QD becomes larger than 10.1 nm, the tube-like curling shows up. We systematically calculate and classify the equilibrium structures of Janus MoSSe QDs with various shapes and edges, as plotted in Fig. 4b. The curling type is primarily dominated by the size of QD, and the transition occurs at the sizes of around 10 nm and 13 nm for hexagonal and triangular MoSSe QDs, respectively. Edge type shows only trivial influence within the considered size range which avoids generating new bonds between edges. For square MoSSe flake, rolled up edges can be perfectly sewed up to form a nanotube [39] if the flake is large enough. In FE model, due to the larger curvature compared with MD results, the sizes of curling type transition reduce to around 7 nm and 10 nm for hexagonal QD and triangular QD, respectively. Moreover, the curvatures of hexagonal QDs are obtained by measuring the position of transition metal atoms on the curled diagonal line, as shown in Fig. 4c. The curvature is clearly determined by

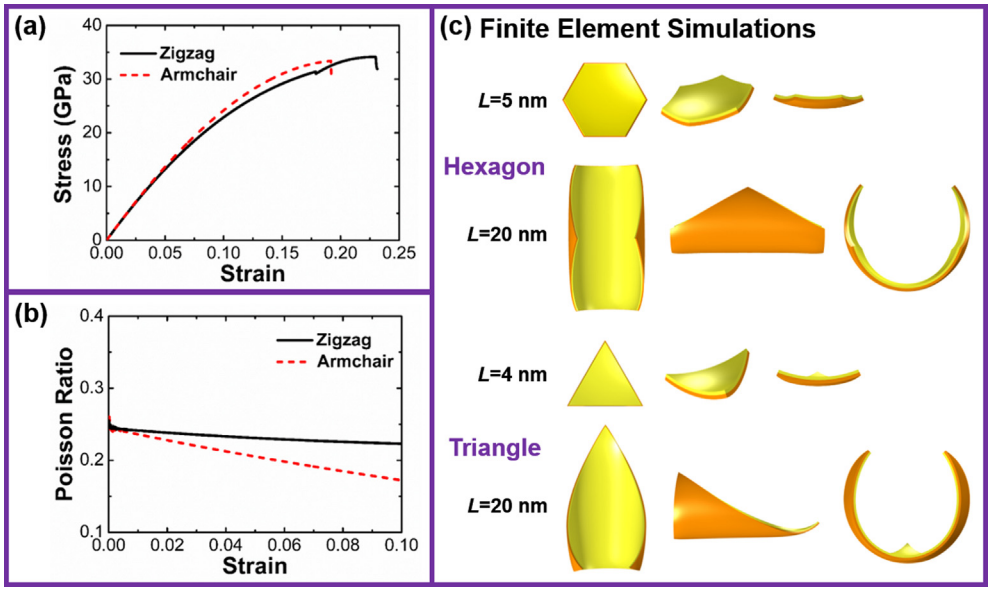

Fig. 3. (a) Uniaxial stress-strain curves of Janus MoSSe monolayer calculated by MD at 0.01 K. (b) Poisson ratio of Janus MoSSe monolayer calculated by MD at 0.01 K. (c) Equilibrium structures of hexagonal and triangle QDs simulated by FE.

the size of QD. In the bowl-like curling region, the curvature linearly decreases with the size of QD. On the contrary, as the increase of size, the curvature increases with a reduced growth rate. Again, the FE analysis reproduces this tendency with higher curvature values.

Since the relaxation of intrinsic strain in Janus TMD QDs acts as the predominant driving force of spontaneous curling, we here demonstrate the impact of misfit on the curvature, taking hexagonal QDs with zigzag edges as an illustrative case. Atomistic models of Janus MoSSe, MoSeTe and MoSTe QDs with the sizes of around 5 nm (576 atoms) and 13 nm (3600 atoms) are built based on the DFT optimized unit cells. We define the misfit in MoXY monolayer as $\varepsilon_{MoXY} = (a_{MoY_2} - a_{MoX_2})/a_{MoY_2}$, where a is lattice constant and X $<$ Y in the chalcogenide period. The values are 0.149, 0.184 and 0.348 nm^{-1} for tube-like curled MoSSe, MoSeTe and MoSTe QDs, respectively. To provide a comparison, we build monolayer Janus TMD nanoribbons to be relaxed in MD as well. The lengths of nanoribbon in zigzag and armchair directions are around 13 nm (40 unit cells) and infinite (periodic boundary condition). In this sense, the nanoribbon will roll up in only zigzag direction which is same as large QD. As shown in Fig. 5a, the curvatures of QDs show a smaller value than those of nanoribbons, which can be attributed to the shape of QD with more flexible free edges. For bowl-like curled QD demonstrated in Fig. 5b, the curvature is smaller than the other two cases and the discrepancy increases with misfit. Overall, the curvatures increase from MoSSe to MoSeTe to MoSTe, confirming the positive correlation between spontaneous curling and misfit.

4. Conclusions

In summary, we perform both molecular dynamics simulations and finite element analysis to investigate the equilibrium structures of hexagonal and triangular Janus MoSSe QDs with various edge types (zigzag and armchair) and sizes. Compared with the initial flat configuration, we observe two distinct types of spontaneous curling (bowl-like and tube-like), which is governed by the size of QD. The transition occurs at the sizes of around 10 nm and 13 nm for hexagonal and triangular MoSSe QDs, respectively. The FE models with equivalent misfit strains qualitatively reproduce the curling behavior, confirming the intrinsic strain in Janus TMDs as the origin of spontaneous curling.

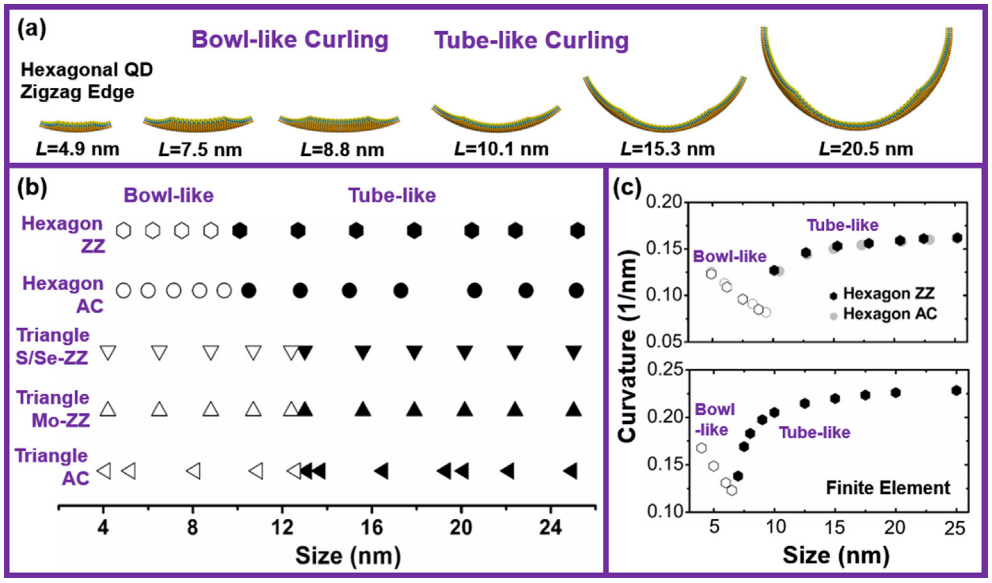

Fig. 4. (a) Equilibrium structures of hexagonal Janus MoSSe QDs with zigzag edges. (b) Curling behavior of Janus MoSSe QD with all considered shapes and edges. Empty (solid) symbols stand for bowl-like (tube-like) curling. (c) Curvature as a function of size of hexagonal QD. MD and FE results are plotted in the upper and lower chart, respectively.

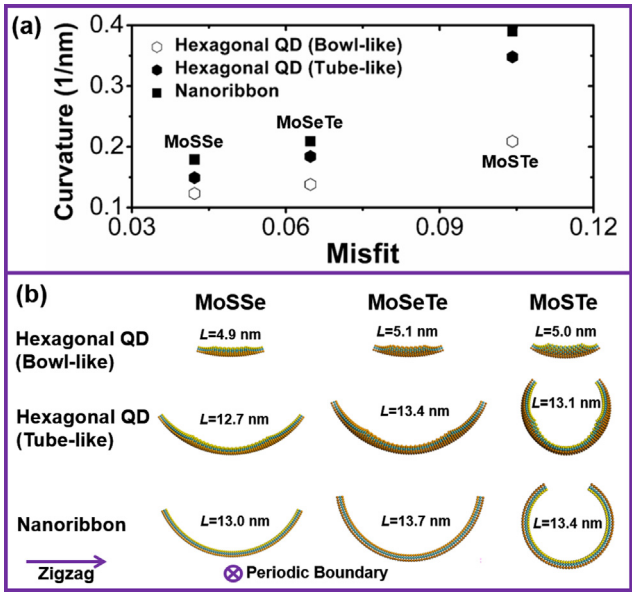

Fig. 5. (a) Curvature as a function of lattice misfit in hexagonal Janus TMD QDs and nanoribbons. (b) Equilibrium structures of hexagonal MoXY QDs and nanoribbons.

Moreover, the dependences of curvature on size and misfit are demonstrated. We expect the theoretical results can help building the foundation for novel nanoscale devices based on Janus TMD QDs.

CRediT authorship contribution statement

Han Ye: Conceptualization, Methodology, Writing - original draft. **Yunzhen Zhang:** Methodology, Software. **Anran Wei:** Software. **Delong Han:** Formal analysis. **Yumin Liu:** Writing - review & editing. **Wenjun Liu:** Supervision. **Yuefeng Yin:** Writing - review & editing. **Mingchao Wang:** Conceptualization, Writing - review & editing.

Declaration of Competing Interest

The authors declare that they have no known competing financial interests or personal relationships that could have appeared to influence the work reported in this paper.

Acknowledgments

This work was supported by the National Natural Science Foundation of China (Grants No. 11974003 and 61671090).

References

[1] S. Manzeli, D. Ovchinnikov, D. Pasquier, O.V. Yazyev, A. Kis, 2D transition metal dichalcogenides, Nat. Rev. Mat. 2 (2017) 17033.
[2] W. Choi, N. Choudhary, G.H. Han, J. Park, D. Akinwande, Y.H. Lee, Recent development of two-dimensional transition metal dichalcogenides and their applications, Mater. Today 20 (2017) 116.
[3] X. Duan, C. Wang, A. Pan, R. Yu, X. Duan, Two-dimensional transition metal dichalcogenides as atomically thin semiconductors: opportunities and challenges, Chem. Soc. Rev. 44 (2015) 8859–8876.
[4] X.P. Ren, L.Q. Pang, Y.X. Zhang, X.D. Ren, H.B. Fan, S.Z. Liu, One-step hydrothermal synthesis of monolayer MoS2 quantum dots for highly efficient electrocatalytic hydrogen evolution, J. Mater. Chem. A 3 (2015) 10693–10697.
[5] T.F. Jaramillo, K.P. Jorgensen, J. Bonde, J.H. Nielsen, S. Horch, I. Chorkendorff, Identification of active edge sites for electrochemical H_2 evolution from MoS_2 nanocatalysts, Science 317 (2007) 100–102.
[6] D. Gopalakrishnan, D. Damien, M.M. Shaijumon, MoS2 quantum dot-interspersed exfoliated MoS2 nanosheets, ACS Nano 8 (2014) 5297–5303.
[7] X. Cao, C. Ding, C. Zhang, W. Gu, Y. Yan, X. Shi, Y. Xian, Transition metal dichalcogenide quantum dots: synthesis, photoluminescence and biological applications, J. Mater. Chem. B 6 (2018) 8011.
[8] T. Wang, H. Zhu, J. Zhuo, Z. Zhu, P. Papakonstantinou, G. Lubarsky, J. Lin, M. Li, Biosensor based on ultrasmall MoS_2 nanoparticles for electrochemical detection of H_2O_2 released by cells at the nanomolar level, Anal. Chem. 85 (2013) 10289–10295.
[9] L. Lin, Y. Xu, S. Zhang, I.M. Ross, A.C.M. Ong, D.A. Allwood, Fabrication of luminescent monolayered tungsten dichalcogenides quantum dots with giant spin-valley coupling, ACS Nano 7 (2013) 8214–8223.
[10] A. Manikandan, Y.Z. Chen, C.C. Shen, C.W. Sher, H.C. Kuo, Y.L. Chueh, A critical review on two-dimensional quantum dots (2D QDs): from synthesis toward applications in energy and optoelectronics, Prog. Quant. Electron. 68 (2019) 100226.
[11] T. Wang, L. Liu, Z. Zhu, P. Papakonstantinou, J. Hu, H. Liu, M. Li, Enhanced electrocatalytic activity for hydrogen evolution reaction from self-assembled monodispersed molybdenum sulfidenanoparticles on an Au electrode, Energy Environ. Sci. 6 (2013) 625–633.
[12] X. Zhao, X. Ma, J. Sun, D. Li, X. Yang, Enhanced catalytic activities of surfactant-assisted exfoliated WS_2 nanodots for hydrogen evolution, ACS Nano 10 (2016) 2159–2166.
[13] M.O. Valappil, A. Anil, M. Shaijumon, V.K. Pillai, S. Alwarappan, A single-step electrochemical synthesis of luminescent WS_2 quantum dots, Chem. Eur. J. 23 (2017) 9144–9148.
[14] K. Zhou, Y. Zhang, Z. Xia, W. Wei, As-prepared MoS2 quantum dot as a facile fluorescent probe for long-term tracing of live cells, Nanotechnology 27 (2016) 275101.
[15] W. Gu, Y. Yan, C. Zhang, C. Ding, Y. Xian, One-Step Synthesis Of Water-Soluble MoS_2 quantum dots via a hydrothermal method as a fluorescent probe for hyaluronidase detection, ACS Appl. Mater. Interfaces 8 (2016) 11272–11279.
[16] D.D.D. Haldar, S.K. Saha, High selectivity in water soluble MoS_2 quantum dots for sensing nitro explosives, J. Mater. Chem. C 4 (2016) 6321–6326.
[17] G.G.D. Han, K.H. Tu, F. Niroui, W. Xu, S. Zhou, X. Wang, V. Bulovic, C.A. Ross, J.H. Warner, J.C. Grossman, Photoluminescent arrays of nanopatterned monolayer MoS_2, Adv. Funct. Mater. 27 (2017) 1703688.
[18] K.H. Ibrahim, M. Irannejad, B. Wales, J. Sanderson, M. Yavuz, K.P. Musselman, Strong exciton-photon coupling in hybrid inorganic-organic perovskite micro/nanowires, Adv. Opt. Mater. 6 (2018) 761.
[19] G. Ou, P. Fan, X. Ke, Y. Xu, K. Huang, H. Wei, W. Yu, H. Zhang, M. Zhong, H. Wu, Y. Li, Defective molybdenum sulfide quantum dots as highly active hydrogen evolution electrocatalysts, Nano Res. 11 (2017) 751–761.
[20] X. Wang, G. Sun, N. Li, P. Chen, Quantum dots derived from two-dimensional materials and their applications for catalysis and energy, Chem. Soc. Rev. 45 (2016) 2239.
[21] Y. Wang, J.Z. Ou, S. Balendhran, A.F. Chrimes, M. Mortazavi, D.D. Yao, M.R. Field, K. Latham, V. Bansal, J.R. Friend, S. Zhuiykov, N.V. Medhekar, M.S. Strano, K. Kalantar-Zadeh, Electrochemical control of photoluminescence in two-dimensional MoS2 nanoflakes, ACS Nano 7 (2013) 10083.
[22] G.C. Loh, R. Pandey, Y.K. Yap, S.P. Karna, MoS2 quantum dot: effects of passivation, additional layer, and h-BN substrate on its stability and electronic properties, J. Phys. Chem. C 119 (2015) 1565–1574.
[23] C. Price, N. Frey, D. Jariwala, V.B. Shenoy, Engineering zero-dimensional quantum confinement in transition-metal dichalcogenide heterostructures, ACS Nano 13 (2019) 8303–8311.
[24] A.Y. Lu, H. Zhu, J. Xiao, C.P. Chuu, Y. Han, M.H. Chiu, C.C. Cheng, C.W. Yang, K.H. Wei, Y. Yang, Y. Wang, D. Sokaras, D. Nordlund, P. Yang, D.A. Muller, M.Y. Chou, X. Zhang, L.J. Li, Janus monolayers of transition metal dichalcogenides, Nat. Nanotech. 12 (2017) 744–749.
[25] J. Zhang, S. Jia, I. Kholmanov, L. Dong, D. Er, W. Chen, H. Guo, Z. Jin, V.B. Shenoy, L. Shi, J. Lou, Janus monolayer transition-metal dichalcogenides, ACS Nano 11 (2017) 8192–8198.
[26] D. Er, H. Ye, N.C. Frey, H. Kumar, J. Lou, V.B. Shenoy, Prediction of enhanced catalytic activity for hydrogen evolution reaction in Janus transition metal dichalcogenides, Nano Lett. 18 (2018) 3943–3949.
[27] W. Shi, G. Li, Z. Wang, Triggering catalytic active sites for hydrogen evolution reaction by intrinsic defects in Janus monolayer MoSSe, J. Phys. Chem. C 123 (2019) 12261–12267.
[28] L. Dong, J. Lou, V.B. Shenoy, Large in-plane and vertical piezoelectricity in Janus transition metal dichalchogenides, ACS Nano 11 (2017) 8242–8248.
[29] G. Kresse, J. Furthmüller, Efficient iterative schemes for ab initio total-energy calculations using a plane-wave basis set, Phys. Rev. B 54 (1996) 11169.
[30] G. Kresse, J. Hafner, Ab initio molecular dynamics for open-shell transition metals, Phys. Rev. B 48 (1993) 13115.
[31] J.P. Perdew, K. Burke, M. Ernzerhof, Generalized gradient approximation made simple, Phys. Rev. Lett. 77 (1996) 3865.
[32] H.J. Monkhorst, J.D. Pack, Special points for Brillouin-zone integrations, Phys. Rev. B 13 (1976) 5188.
[33] X. Ma, X. Wu, H. Wang, Y. Wang, A Janus MoSSe monolayer: a potential wide solar-spectrum water-splitting photocatalyst with a low carrier recombination rate, J. Mater. Chem. A 6 (2018) 2295–2301.
[34] A. Togo, I. Tanaka, First principles phonon calculations in materials science, Scripta Mater. 108 (2015) 1–5.
[35] S. Baroni, S. De Gironcoli, A. Dal Corso, P. Giannozzi, Phonons and related crystal properties from density-functional perturbation theory, Rev. Mod. Phys. 73 (2001) 515.
[36] H. Ye, J. Zhou, D. Er, C.C. Price, Z. Yu, Y. Liu, J. Lowengrub, J. Lou, Z. Liu, V.B. Shenoy, Toward a mechanistic understanding of vertical growth of van der Waals stacked 2D materials: a multiscale model and experiments, ACS Nano 11 (2017) 12780.
[37] S. Plimpton, Fast parallel algorithms for short-range molecular dynamics, J.

Comput. Phys. 117 (1995) 1–19.
[38] J.W. Jiang, Misfit strain induced buckling for transition-metal dichalcogenide lateral heterostructures: a molecular dynamics study, Acta Mech. Solida Sinica 32 (2018) 17–28.
[39] Q.L. Xiong, J. Zhou, J. Zhang, T. Kitamurad, Z.H. Li, Spontaneous curling of free-standing Janus monolayer transition-metal dichalcogenides, Phys. Chem. Chem. Phys. 20 (2018) 20988–20995.
[40] W.G. Hoover, Canonical dynamics: equilibrium phase-space distributions, Phys. Rev. A 31 (1985) 1695.
[41] A. Castellanos-Gomez, M. Poot, G.A. Steele, H.S.J. van der Zant, N. Agraït, G. Rubio-Bollinger, Elastic properties of freely suspended MoS2 nanosheets, Adv. Mater. 24 (2012) 772–775.